Microporous and Mesoporous Materials 224 (2016) 323–331

Contents lists available at ScienceDirect

Microporous and Mesoporous Materials

journal homepage: www.elsevier.com/locate/micromeso

A comparative study of several microporous materials to store methane by adsorption

Andrés A. García Blanco [a], Andrea F. Vallone [a], Sophia A. Korili [b], Antonio Gil [b], Karim Sapag [a, *]

[a] Laboratorio de Sólidos Porosos, INFAP, CONICET – Universidad Nacional de San Luis, Chacabuco, 917, 5700, San Luis, Argentina
[b] Departamento de Química Aplicada, Universidad Pública de Navarra, Edificio Los Acebos, Campus de Arrosadia, E-31006, Pamplona, Spain

ARTICLE INFO

Article history:
Received 22 July 2015
Received in revised form
4 December 2015
Accepted 4 January 2016
Available online 9 January 2016

Keywords:
Methane adsorption
Microporous materials
Isosteric enthalpy of methane adsorption
Adsorbed natural gas (ANG)

ABSTRACT

Methane adsorption was studied in microporous materials with differences in their pore geometry and surface chemistry in order to evaluate the characteristics that enhance methane storage in porous materials. The studied materials included metal-organic frameworks (Cu-BTC, MIL-53 and ZIF-8), zeolites (5A and 13X) and an activated carbon (Maxsorb). Textural properties such as pore volume and specific surface area were studied by nitrogen adsorption–desorption isotherms. Methane adsorption was analyzed by means of measurements at low and high pressures (0–5000 kPa) at various temperatures (278–323 K). The effect of the adsorbate–adsorbent interaction was evaluated by the determination of the Henry constant using the adsorption data of methane at low pressures and 298 K. In addition, the isosteric enthalpy of adsorption using data of adsorption at several temperatures was obtained. A linear trend was observed between the Henry constant, the enthalpy of adsorption and the pore size, indicating that the latter is the most influential factor in the interaction of a microporous adsorbent and methane at room temperature. Also, it was found that the textural properties (i.e. specific surface and micropore volume) are directly related with the methane storage capacity at 298 K and 3.5 MPa. However, we obtained a deviation of this behavior for ZIF-8 that is related to its geometry and pore size.

1. Introduction

The need for alternative energy sources that replace the current petroleum-derived fuels has attracted attention to the study of new clean fuels with lower atmospheric emissions and higher availability than conventional petroleum. Hydrogen and natural gas (NG) are two of the alternative fuels evaluated, which have the common characteristic of being gaseous at room temperature, a fact that introduces difficulties for their transport and storage. Porous materials have been considered as an alternative to store these gases by adsorption; in a previous work we presented the behavior of several microporous materials to store hydrogen [1].

In reference to NG, it is known that it is a non-renewable resource, but developments made in the extraction of shale gas have increased substantially the availability of this fuel. Also, it provides a clean and efficient combustion, with lower emissions of sulfur, lead oxides, benzene and solid particles than conventional petroleum derivatives such as gasoline and diesel [2,3]. The use of porous materials to store methane by adsorption, by means of the so-called adsorbed natural gas (ANG) technology, consider materials with elevated surface areas to store high amounts of gas at lower pressures than the conventional compressed natural gas technology (CNG). Since methane is the main component of natural gas, many of the previous studies related to ANG have focused on the study of methane adsorption at pressures up to 3500 kPa and room temperature. Mainly, it has been evaluated the use of microporous materials, such as zeolites [4–6] and activated carbons [4,7–12]. An important reason for the use of these kinds of materials is the elevated adsorptive potential in the micropores, due to the overlapping of pore wall potentials. These elevated potentials are important to confine high quantities of gas molecules, and based on this fact, previous studies have evaluated the effect of pore size and geometry in methane storage capacities of porous materials.

In recent years, developments made in the synthesis of tailored porous materials, such as metal-organic frameworks (MOF), have

* Corresponding author.
E-mail address: sapag@unsl.edu.ar (K. Sapag).

http://dx.doi.org/10.1016/j.micromeso.2016.01.002
1387-1811/

elevated the number of materials which could be used to store methane [13,14]. Furthermore, some novel effects are discussed, for example, the effect of specific adsorption sites, which could enhance methane adsorption [15,16].

The Department of Energy of the United States (DOE) has issued a call for the development of materials capable of achieving volumetric and gravimetric capacities > 12.5 MJ/dm^3 (314.2 v_{CH_4} (STP)/$v_{sorbent}$) and >0.5 $g_{CH_4}/g_{sorbent}$ (700 cm^3 CH_4 (STP)/$g_{sorbent}$) respectively, at reasonably pressure and temperature ranges (from 233 to 358 K and 3500 kPa) in order to achieve targets of >9.2 MJ/dm^3 and >0.4 $g_{CH_4}/g_{sorbent}$ in an ANG fuel storage system [2].

The properties of porous materials, which can be modified in order to optimize their gas storage capacity, are mainly addressed to the adsorbent–adsorbate interaction, geometry and size of their pores. Another important property that should be optimized to enhance the volumetric gas storage capacity of porous materials is their apparent density. This property has been studied in previous works [7,17,18] and is out of the scope of this study.

The aim of this work is to perform a comparative study among porous materials with differences in their chemical nature, pore size and geometry. There were studied the characteristics of methane adsorption in a series of microporous materials with various physicochemical characteristics. The selected materials were, three MOF, two zeolites and an activated carbon. The focus of the work is to compare the effect of factors such as pore size and geometry and adsorbent–adsorbate interaction. For this purpose, it was performed a characterization by means of nitrogen adsorption–desorption isotherms at 77 K, a technique that allows obtaining textural parameters of importance in the study of gas storage, such as the pore size distribution, the micropore volume and the specific surface area. The study of methane adsorption in the selected materials was performed by means of methane adsorption isotherms at low and high pressures (up to 5.0 MPa) and various temperatures. In order to evaluate the adsorbent–adsorbate interaction, the Henry constants and the isosteric enthalpy of adsorption were evaluated. The Henry constants were determined from low pressure adsorption isotherms and the isosteric enthalpy of adsorption was calculated by means of the Clausius–Clapeyron equation applied to high pressure adsorption data at several temperatures. It is also discussed the role of the adsorbed phase volume and the adsorbed phase density, since these factors are important in the study of adsorption above the critical temperature (T_c).

The correlation between textural properties and methane adsorption at conditions of storage in an ANG tank (3500 kPa and 298 K) are discussed as well as the desired characteristics of an adsorbent which could be used to store this gas.

2. Experimental

2.1. Materials

2.1.1. Metal-organic frameworks

Basolite™ C300 is the trademark of Sigma Aldrich for the Cu-BTC (BTC stands for benzene-1,3,5-tricarboxylate) MOF. This MOF was first reported by Chui et al. [19] as HKUST-1. The pore network of Cu-BTC has two kinds of pores; the main channels of the tridimensional network have a square cross-section of ca. 1.0 nm diameter and tetrahedral side pockets of ca. 0.5 nm [19–21]. One of the special characteristics of the Cu-BTC is that upon vacuum heating, the material loses the axial aqua ligands and leaves the Cu^{2+} ions exposed [20,21].

Basolite™ A100 is the trademark of Sigma Aldrich for the MIL-53 MOF. This MOF has a structure built up from infinite chains of corner-sharing $MO_4(OH)_2$ (in the case of Basolite A100 M = Al^{3+}) octahedral interconnected by the dicarboxylate groups [22,23]. This structure results in a 3D metal organic framework containing one single pore size with 1D diamond shaped channels with pores of free diameter close to 0.85 nm [24]. However, the MIL-53 has shown reversible structural changes due to the framework interaction with guest molecules, reported as a “breathing effect” of the pores. Initially this “breathing effect” was reported for the hydration–dehydration of the MIL-53 [22,23], but latter was found in the interaction with adsorbates like CO_2 [24].

Basolite™ Z1200 is the trademark of Sigma Aldrich for the ZIF-8 material. ZIF (zeolitic imidazolate frameworks) materials are a subfamily of the MOF materials in which the crystalline structures composed of metal ions and organic linkers are ordered in an analogous fashion to that of silicon and oxygen in zeolites. ZIF-8 is composed of $Zn(MeIM)_2$ (MeIM = 2-methylimidazolate) with a sodalite-type structure, exhibiting an interesting nanopore topology formed by four-ring and six-ring ZnN_4 clusters with nanopores accessible through narrow six-ring funnel-like channels [25–27]. The internal cavities of this material have an approximate diameter of 1.16 nm and the pore aperture diameter is of 0.34 nm [25].

2.1.2. Zeolites

The zeolites employed in this work were molecular sieves 5A and 13X. Zeolites are crystalline materials made up of silicon, aluminum and positive ions which are added to balance the molecule.

The structure of zeolites A consist of eight sodalite cages located at the corners of a cube and joined through four-membered oxygen ring (S4R). This arrangement forms a large polyhedral α cage of free diameter about 1.14 nm accessible through eight-membered oxygen windows. Stacking these units in a cubic lattice gives a three-dimensional isotropic channel structure, constricted by eight-membered oxygen rings [28]. Zeolite 5A is the calcium form of molecular sieves and presents a pore size close to 0.5 nm (which corresponds to the size of the pore window).

Zeolites X present a Faujasite framework structure. The framework may be thought of as a tetrahedral lattice of sodalite units connected through six-membered oxygen bridges, or equivalently as a tetrahedral arrangement of double six-ring units. The resulting channel structure is very open, with each cage connected to four other cages through twelve-membered oxygen rings of free-diameter around 0.74 nm. The Si/Al ratio in zeolite is 1–1.5 and gives to the structure five different cation sites [28]. 13X is a sodium-modified molecular sieve, with a pore window diameter around 0.74 nm.

2.1.3. Carbon materials

The high surface area activated carbon is commercialized by Kansai Coke and Chemicals as Maxsorb. Activated carbons are characterized for being non-crystalline solids with slit pore geometry between two graphene layers [29].

2.2. Adsorption measurements

N_2 (Linde, 99.999% purity) adsorption–desorption isotherms and low pressure methane (Linde, 99.995% purity) adsorption isotherms were measured in automatic manometric systems Autosorb AS-1MP (Quantachrome Instruments) and ASAP 2000 (Micromeritics Instrument Corporation). High pressure adsorption isotherms of methane (Linde, 99.995% purity) were measured at various temperatures (278–323 K) in a high pressure manometric system HPA 100 (VTI Corporation, currently TA Instruments).

Previous to all the adsorption experiments, the samples were degassed for 12 h under vacuum conditions (7×10^{-4} kPa). The

activated carbon was degassed at 523 K, zeolites at 573 K, the Cu-BTC and MIL-53 at 473 K, and ZIF-8 at 373 K.

3. Results and discussion

3.1. N_2 adsorption–desorption isotherms

Nitrogen adsorption–desorption is one of the most employed methods of characterization of porous materials. The experimental adsorption–desorption isotherms of nitrogen at 77 K of the materials selected for this study are shown in Fig. 1. It can be appreciated that all the isotherms at low pressures correspond to the type I, according to the classification of the IUPAC [30], indicating the microporous character of all the materials. The results for MIL-53 present a deviation from the mentioned type of isotherm, with a marked increase in adsorption at high relative pressures.

The samples were studied in its pelletized form, thus the increase at high relative pressures could be due to condensation in large pores (due to pellet shaping). The adsorption–desorption isotherm of the activated carbon shows a broad knee at relative pressures minor than 0.2 indicating the presence of super-micropores in this sample.

MOFs and zeolites have ordered (crystalline) structures with definite pore sizes, whereas the activated carbon is an amorphous material with a disordered structure and a distribution of pore sizes of less than 3 nm, as is shown in the pore size distribution (PSD) reported previously [1].

The textural properties that characterize microporous materials are the specific surface calculated with the BET equation (S_{BET}) and the micropore volume, which can be calculated with various models applied to the adsorption of vapors on solids [31,32]. The calculated textural parameters are shown in Table 1, where the micropore volume is calculated using Dubinin-Radushkevich (DR) and Dubinin-Astakhov (DA) equations (V_o DR and V_o DA, respectively).

In addition, CO_2 has been reported to be a useful tool in the characterization of narrow microporosity (pores smaller than 0.7 nm) of activated carbons [33]. CO_2 adsorption (isotherm not shown) was measured in order to obtain the volume of narrow micropores (V_{DR} CO_2) of Maxsorb sample. The obtained value (0.49 cm^3 g^{-1}) is lower than the volume of micropores obtained from N_2 adsorption, that is in accordance with the PSD of this sample, which indicates that not only narrow micropores are present, but also there is an important contribution of pores between 0.7 and 2.0 nm.

Table 1
Textural properties of the materials studied, calculated from N_2 adsorption–desorption isotherms at 77 K.

	S_{BET} [m^2 g^{-1}]	C_{BET}	V_o DR [cm^3 g^{-1}]	V_o DA [cm^3 g^{-1}]
Cu-BTC	888	24,500	0.32	0.32
MIL-53	837	7430	0.32	0.31
ZIF-8	1890	1150	0.74	0.74
5A	613	14,200	0.22	0.22
13X	725	15,000	0.26	0.26
Maxsorb	3090	140	1.02	0.98

3.2. Methane adsorption

3.2.1. High-pressure methane adsorption isotherms

The high-pressure adsorption isotherms of methane in the studied materials at various temperatures (between 278 and 323 K) are shown in Fig. 2.

The temperatures of methane adsorption isotherms measured are all above the T_c of methane (191 K). This fact indicates that the mechanism of pore filling in this adsorption studies could be different than the one of vapors (below their T_c). The main characteristic of adsorption of gases above their T_c is the absence of condensation. In fact, one of the main difficulties in the study of gas adsorption above T_c is the determination of the adsorbed phase density (ρ_{ads}) and the volume of the adsorbed phase (V_{ads}) [34] while in the adsorption of gases below their T_c, the adsorbed phase density is assumed to be equal to the density of the adsorbible in its liquid state [31].

These parameters define the absolute amount adsorbed (n_{abs}), since experimental data correspond to excess quantities. The relationship is given by the equation:

$$n_{abs} = n^{\sigma} + \rho_{bulk} V_{ads} \tag{1}$$

where n^{σ} corresponds to the excess adsorption (in mmol per gram of solid), ρ_{bulk} is the density of the fluid in the bulk (in mmol per cm^3), and V_{ads} is the volume of the adsorbed phase (in cm^3 per gram of solid).

Also, the V_{ads} and ρ_{ads} are related by the equation

$$V_{ads} = \frac{n^{\sigma}}{\rho_{ads} - \rho_{bulk}} \tag{2}$$

There are various strategies reported to calculate n_{abs}, some of them are based on determining V_{ads} and others in determining ρ_{ads} by using different assumptions or approximations [34–37].

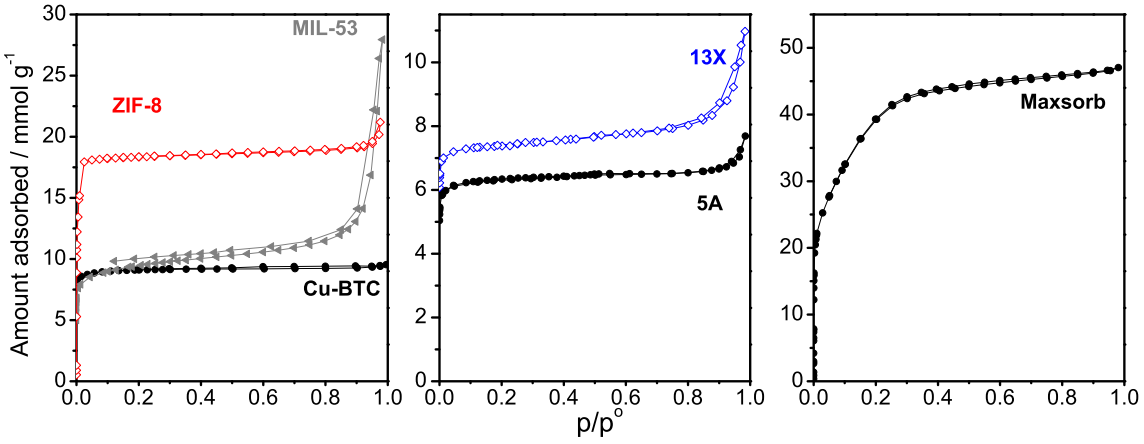

Fig. 1. Nitrogen adsorption–desorption isotherms at 77 K.

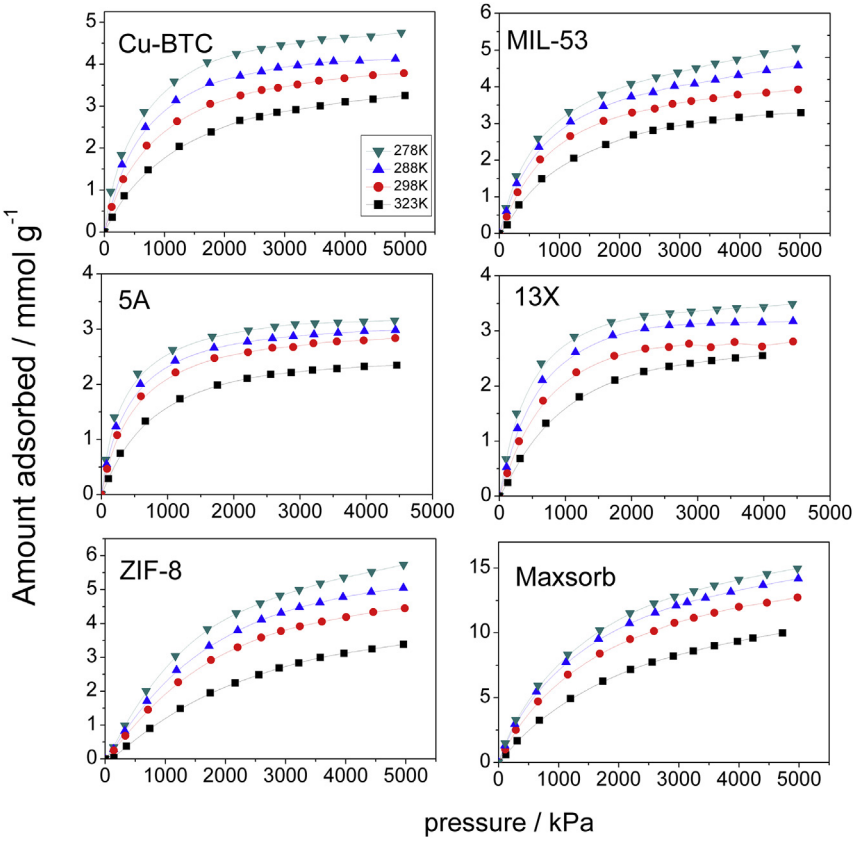

Fig. 2. High pressure adsorption isotherms of methane at various temperatures. Symbols correspond to experimental excess data, continuous lines are a guide to the eye.

Analyzing the values of ρ_{ads} reported in bibliography, many of them report that the density of adsorbed methane (at temperatures above 273 K) is considerable minor than the density of liquid methane (0.47 g/cm^3), with values ranging between 0.23 and 0.27 g/cm^3 for activated carbons [34,38–42]. However, some authors have reported values close to the density of the liquid methane (0.44 g/cm) [37], showing the wide range of reported values for this parameter.

Rodriguez-Reinoso et al. [41] reported the use of the characteristic curve of adsorption derived from Dubinin's theory of volume filling of micropores to estimate the density of methane adsorbed in activated carbons at 298 K. Also, Alcañiz-Monge et al. [38] reported that methane adsorption at supercritical conditions on activated carbons with homogeneous narrow PSD follow a mechanism of pore filling which agrees with the characteristic curve of adsorption of N_2 and CO_2, considering a ρ_{ads} of 0.27 g/cm^3. However, they observed that the assumed value of 0.27 g/cm^3 does not fit the N_2 and CO_2 characteristic curves in samples with a wide PSD, because the ρ_{ads} seems to differ with the pore size in microporous materials. In this work, a methodology similar to the one reported by Rodriguez-Reinoso et al. [41] was applied in order to fit the characteristic curves of N_2 and CH_4 adsorption (also CO_2 adsorption isotherm data were used for the Maxsorb sample).

In order to obtain ρ_{ads} using the characteristic curves (CC) methodology, it is used the concept of the characteristic curve reported by Dubinin [43], which assumes that the characteristic curves of adsorption of an adsorbible at different temperatures should be equal. Hence, the plot of ln V_{liq} (where V_{liq} is the amount adsorbed expressed as its volume in liquid phase) as a function of the adsorption potential $A = RT/\ln(f^o/f)$ (where R is the gas constant, T the temperature, f the fugacity of the system and f^o the saturation fugacity) should be independent of the temperature.

Also, when the value of the affinity coefficient (β) is included, a general characteristic curve for a given adsorbent should be obtained, which is the same for all the adsorbibles used. In the methodology used in this study, some modifications were made in order to obtain the characteristic curves of adsorption of a gas above its T_c, since at these conditions f^o and V_{liq} are not defined. These modifications have been previously reported by Alcañiz-Monge et al. [38]. They consider f^o as the fugacity where the compressibility factor is minimum (using the RefProp software we determined that $f^o_{CH_4} = 23.7$ MPa at 278 K, $f^o_{CH_4} = 24.9$ MPa at 288 K, $f^o_{CH_4} = 26.0$ MPa at 298 K and $f^o_{CH_4} = 27.6$ MPa at 323 K) and the affinity coefficients (β) were calculated from interaction parameters which are derived from the Lennard–Jones interaction between the surface and the adsorbed gas. The fact that all the isotherms should coincide into the same characteristic curve is used to determine the value of ρ_{ads} for methane. Various values of ρ_{ads} were tested and the corresponding V_{ads} were calculated using equation (2). Several attempts were made until the obtained characteristic curves at the different temperatures coincide. N_2 adsorption data were included in the characteristic curves, in order to use them as a reference to adjust methane data. The value of ρ_{ads} used for N_2 at 77 K was 0.808 g/cm and 1.023 g/cm for CO_2 at 77 K [38]. From the obtained values of ρ_{ads} using the characteristic curve approximation, the V_{ads} is calculated using equation (2), and the calculated values are also shown in Table 2.

The characteristic curves obtained are shown in Fig. 3, and the values of ρ_{ads} determined by this methodology (ρ_{ads} (CC)) are shown in Table 2 and compared with the ρ_{ads} obtained if it is

Table 2
Volume of the adsorbed phase of methane at 298 K and 3500 kPa and percentage of micropore filled with methane, compared to the micropore volume of the samples.

	ρ_{ads} (CC) [g cm^{-3}]	ρ_{ads} (V_o DA) [g cm^{-3}]	V_{ads} (CC) [cm^3 g^{-1}]	% Micropore filling at 3500 kPa and 298 K
Cu-BTC	0.23	0.19	0.28	88
MIL-53	0.25	0.20	0.26	84
ZIF-8	0.16	0.10	0.47	64
5A	0.23	0.21	0.22	100
13X	0.20	0.17	0.26	100
Maxsorb	0.34	0.16	0.58	59
				118*

* % micropore filling respect to the V_0 DR-CO2.

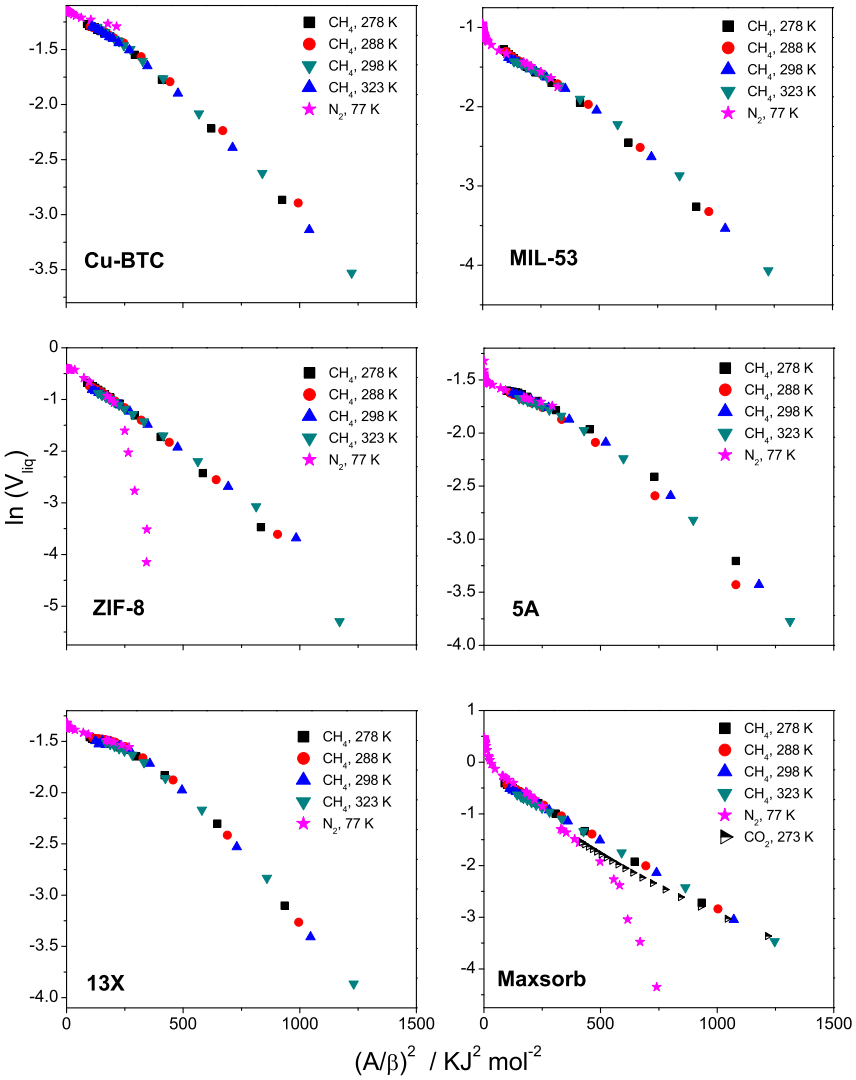

Fig. 3. Characteristic curves of the materials studied, including data of N_2 and CH_4 adsorption (also includes CO_2 adsorption data for the Maxsorb sample).

considered that $V_{ads} = V_o$ DA. The latter could be considered as a good approximation of V_{ads} in samples with definite micropore sizes.

In Fig. 3, some deviations in the characteristic curves are observed in the adsorption data of N_2 in samples ZIF-8 and Maxsorb. These deviations are observed at the lowest pressures of the isotherms and could be attributed to a lack of equilibrium at the conditions of analysis. The CO_2 adsorption (at 273 K) data were included in the characteristic curve of the Maxsorb sample and it can be appreciated that it coincides with the tendency of nitrogen and methane adsorption data.

With the obtained values of V_{ads} (CC), an analysis of the fraction of micropore filling in methane adsorption can be made. This analysis is of importance in the study of the capacity to store methane of a material. In order to calculate the fraction of micropores filled with methane at the expected conditions of an ANG tank, the V_{ads} of methane adsorption isotherms (at 298 K and 3500 kPa) is compared with the V_o DA calculated from N_2 adsorption at 77 K and reported as the percentage of micropore filling in Table 2.

It can be appreciated that for the samples 5A, 13X, Cu-BTC and MIL-53, the micropore fillings are above the 80%, indicating that the

adsorbed phase of methane is occupying almost all the micropores of these materials at 3500 kPa and 298 K. Also, it is interesting that the ρ_{ads} determined by the characteristic curve method for these materials are between 0.20 and 0.25 g/cm^3, showing that the ρ_{ads} of CH_4 at the conditions studied is minor than the ρ_{ads} at the liquid state. Also, it was obtained that the micropore fillings of 5A and 13X samples are of the 100%, a result that is consistent with the experimental isotherms of these samples shown in Fig. 2, where it can be observed that the isotherms are in a plateau which indicates the saturation of the available sites for adsorption.

ZIF-8 and Maxsorb samples present micropore fillings of 64% and 59%, respectively. These values are assigned to different factors, because of the differences in the properties of these materials. The main differences between these materials are the pore sizes and geometry. The activated carbon presents a pore size distribution with pores between 0.5 and 3 nm, while the ZIF-8 has a crystalline structure with definite pore sizes. The pore geometries also differ for these materials (the activated carbon has pores with slit-like geometry and the ZIF-8 has spherical cavities). In the case of the Maxsorb sample, due to the presence of pores with different sizes, some of them could be filled with adsorbed methane, while others (with the largest sizes) could only be partially filled at the conditions studied, and this could be the reason that the micropore filling is only of the 59%. In this sense, is important to highlight that the micropore filling calculated with respect to the V_o-DR-CO_2 for the Maxsorb sample is higher than 100%, indicating that methane is not only adsorbed in the narrowest micropores (pore size < 0.8 nm). Instead, it indicates that micropores with sizes larger than 0.8 nm are important in methane adsorption at room temperature. Similar results have already been highlighted by Rodriguez-Reinoso et al. [41].

The case of ZIF-8 sample is different, since it presents an ordered structure with uniform pore sizes. Then, the 64% of micropore filling indicates that the pores of this sample are partially filled with a ρ_{ads} of 0.16 g/cm^3, indicating that in this material methane is not especially adsorbed at the studied conditions. This behavior could be attributed to the textural properties of these materials, especially to the pore size and geometry (the spherical internal cavity and its narrow pore aperture). Considering that previous studies have reported that pore sizes around 1.1 nm in pores with slit geometry are optimal for methane storage [44,45], the fact that ZIF-8 has pores with spherical geometry with a diameter of 1.16 nm, indicates that its pore geometry and its narrow pore aperture are probably responsible for the low ρ_{ads} and low micropore filling of adsorbed methane in this sample.

3.2.2. Evaluation of the adsorbent–adsorbate interaction and the isosteric enthalpy of adsorption

The adsorbent–adsorbate interaction is an important property in the characterization of gas adsorption over porous solids, and with relevance to the design of porous materials for gas storage. However, it is not easy to determine reliable parameters to study this property. The Henry constant (H) is a characteristic parameter of the adsorption isotherms at very low pressures and is an important parameter to study the adsorbate–adsorbent interaction [46,47].

Low pressure methane adsorption isotherms were measured at 298 K (Fig. 4) and the Henry constant was obtained from the linear region at the lowest pressures. It should be mentioned that usually H cannot be determined experimentally because the linear region in adsorption isotherms is rarely observed. However, in Fig. 4 is shown that the measured isotherms of adsorption of methane present linear behaviors at the pressures studied, due to the high T/T_o in which the experiments were performed. In the case of the MOF, the isotherms present some deviations from linearity, and in such cases, the initial linear data points at the lowest pressures were considered to determine H.

In addition, with the adsorption isotherms at high pressures and various temperatures, the isosteric enthalpy of adsorption at different coverage can be obtained using the Clausius–Clapeyron equation [48]:

$$\Delta_{ads}h_{n^\sigma} = R\cdot\left(\frac{\partial \ln[P]}{\partial(1/T)}\right)_{n^\sigma} \quad (3)$$

where R is the gas constant, and $\Delta_{ads}h_{n^\sigma}$ is calculated from plots of log pressure, ln [P], for a given amount adsorbed n^σ as a function of reciprocal temperature, $1/T$. It has been previously reported [48] that due to the sensitivity of this methodology to errors in pressure measurements; the values of $\Delta_{ads}h_{n^\sigma}$ at low pressures (or surface coverage) are better determined with calorimetric methods than with the isosteric method. However, at high pressures, the calorimetric methods become less precise, and the isosteric method is adequate. The obtained $\Delta_{ads}h_{n^\sigma}$ at several loading for the materials studied are shown in Fig. 5.

In spite of not possessing a dipolar or quadrupole moment which could interact with charged sites in the surface of the materials, methane could be preferentially adsorbed in charged sites due to its polarizability. In the case of Maxsorb sample, it is observed a decrease in the $\Delta_{ads}h_{n^\sigma}$ as a function of the amount adsorbed, due to the surface heterogeneity which arises from the PSD that characterizes this material (pores with the smallest sizes present the highest adsorption energies). At high amounts adsorbed, the $\Delta_{ads}h_{n^\sigma}$ obtained for Maxsorb is close to the values obtained by molecular simulation [49] for pores with sizes around 1.0 nm (around 2–2.5 times the molecular diameter of methane).

The results shown in Fig. 5 are comparable with the values of adsorption enthalpy reported for the adsorption of methane in Cu-BTC (values between 18 and 20 kJ/mol obtained from experimental data and molecular simulations [2,16,37,50]) and MIL-53 (~17 kJ/mol, determined by adsorption microcalorimetry [24]). The value obtained for the ZIF-8 sample is slightly higher than the reported value of ~12 kJ/mol obtained by Zhou et al. [51].

The relation between H and $\Delta_{ads}h_{n^\sigma}$ with the pore size of the materials is presented in Fig. 6. It should be mentioned that in the case of Cu-BTC the pore size of the "pockets" of 0.5 nm was considered; and for the zeolites the size of the "pore window" was considered (0.5 and 0.74 for 5A and 13X, respectively), instead of the size of the internal cavity. Also, the value of $\Delta_{ads}h_{n^\sigma}$ at the lowest amount adsorbed measured was selected for the correlation.

It is observed that both H and $\Delta_{ads}h_{n^\sigma}$ follow a similar tendency, increasing with the decrease of the pore size, as is expected due to the increase in the adsorption potential. However, the values of H of the zeolites are deviated of the tendency observed, showing higher values than expected. This deviation could be related to the surface properties of the zeolites, more specifically to the electrostatic charges of their surface, in spite of the fact that methane has neither dipolar nor quadrupole moment. Previous studies have correlated the surface characteristics of zeolites 5A and 13X with the adsorption enthalpies of hydrocarbons, and found that the latter increases with the acidic character of the adsorbent [52]. Then, the deviations observed could be attributed to an increase of the adsorbent–adsorbate interaction of methane in zeolites, indicating that the adsorbent–adsorbate interaction seems to be enhanced in samples which present sites with electrostatic charges.

In Fig. 6, Maxsorb sample was not included because of the different pore sizes that it presents. However, it should be mentioned that the value of H determined for this sample was the highest, probably due to the narrowest pores present in this sample, which possess a broad pore size distribution.

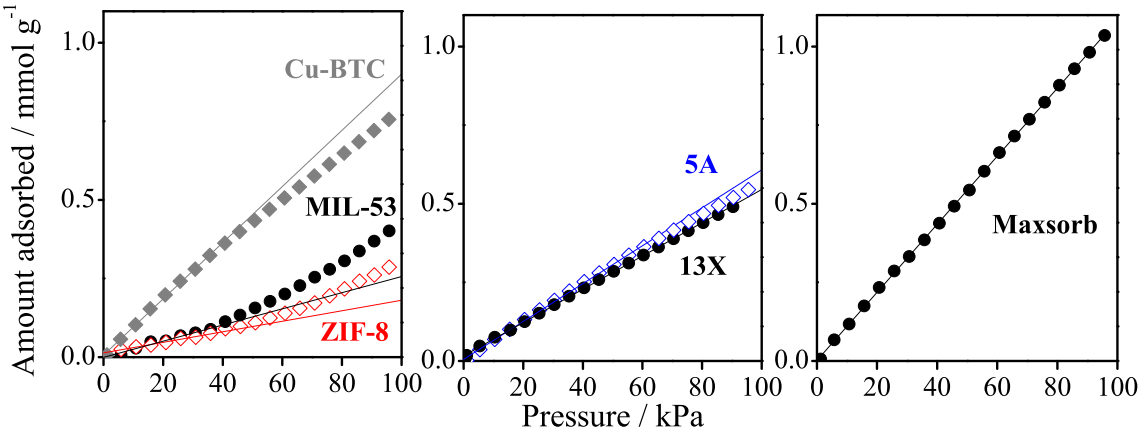

Fig. 4. Low pressure methane adsorption isotherms at 298 K.

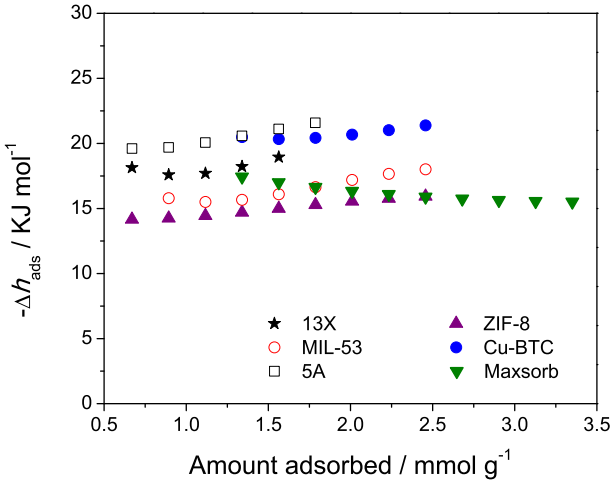

Fig. 5. Isosteric enthalpy of adsorption as a function of the amount adsorbed, calculated using the Clausius–Clapeyron equation.

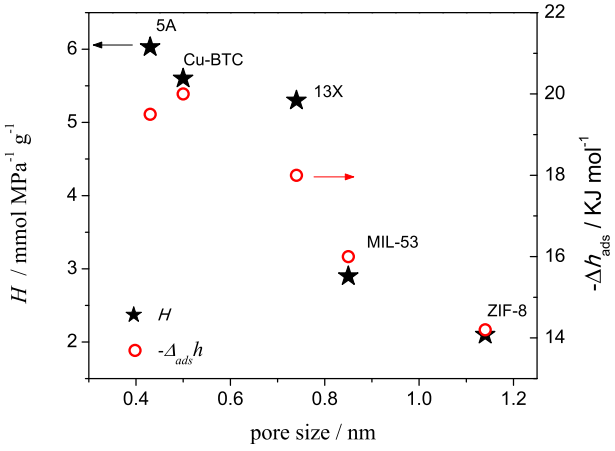

Fig. 6. Correlation between the pore size and the adsorbent–adsorbate parameters (H and $-\Delta h_{ads}$).

3.2.3. Correlation between the textural parameters and the methane storage capacity at 3500 kPa

Finally, it is discussed the correlation between the textural properties of the materials with the adsorption of methane at 3500 kPa and 298 K. In previous studies, a linear correlation between surface area and micropore volume with the adsorption of methane has been reported, and this correlation is considered a useful tool for the estimation of the methane storage capacity of a material using N_2 adsorption data [2,4,7,10,53,54]. However, some deviations are observed that usually are not discussed. In this work, it has been observed that, in spite of the fact that all the materials studied are essentially microporous, they present differences in their pore sizes and in their adsorbate–adsorbent interactions. Results indicated that Cu-BTC and zeolites (5A and 13X) present the highest adsorbate–adsorbent interaction, whereas ZIF-8 presents the lowest values of H and $\Delta_{ads}h_{n^{\sigma}}$. Also, there were observed differences in the values of the adsorbed phase density of methane and the micropore filling at 3500 kPa and 298 K.

In Fig. 7, is observed that methane adsorption capacity at 3500 kPa and 298 K of ZIF-8 is deviated from the tendency followed by the other samples studied (zeolites, Cu-BTC, MIL-53 and Maxsorb). This deviation indicates that the adsorption capacity of methane in this sample, at the conditions mentioned is lower than the one expected from their textural properties (S_{BET} and V_o DA) determined from N_2 adsorption at 77 K. From the different parameters evaluated in this study, it was observed that methane in ZIF-8 presented the lowest value of ρ_{ads} of methane at 298 K, and the lowest adsorbate–adsorbent parameters. Then, it could be said that the surface properties of ZIF-8 (both the geometry and size of its pores and the affinity towards methane molecules) might not be favorable for the storage of methane at 3500 kPa and 298 K. However, it presents the second highest methane adsorption capacity, indicating that its adsorption capacity is high. In fact, the shapes of the isotherms are representative of the low adsorbent–adsorbate interaction, which is important when determining the delivery capacity of the material, which corresponds to the volume of gas discharged up to a residual pressure of 0.1 MPa.

Finally, as it was mentioned in the introduction, in this paper we do not deal with the V/V storage capacities of the materials. However, it is important to mention that this issue is one of the most important in the development of materials for methane storage. For example, Maxsorb sample, despite having the highest gravimetric adsorption capacities, presents a low density that lowers its V/V capacity. A recent report [55] has analyzed this fact, indicating the importance of Cu-BTC as one of the materials which present a good relation between its methane storage capacity and its density.

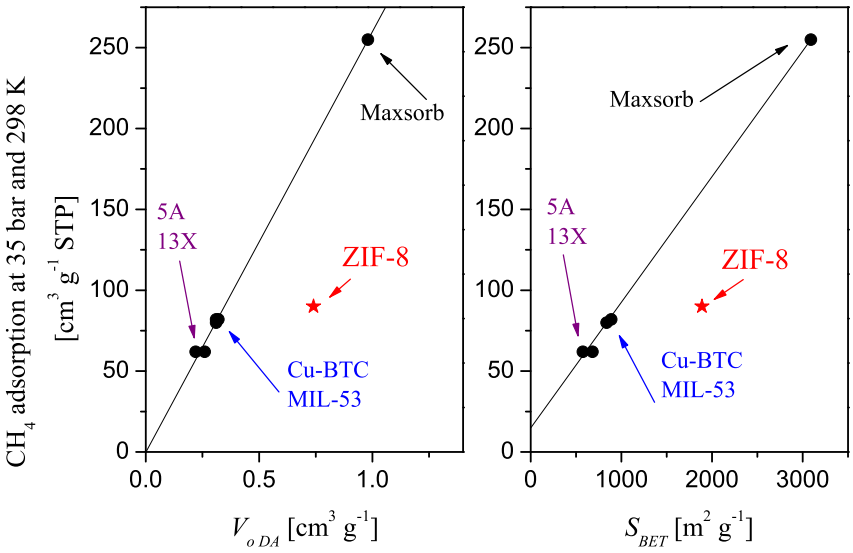

Fig. 7. Correlation between surface area and micropore volume with methane storage capacity of microporous materials.

4. Conclusions

The characteristics of methane adsorption in a series of microporous materials with different pore geometry, surface chemistry and pore size were studied. Low and high-pressure adsorption isotherms of CH_4 were used for the determination of parameters such as the density of the adsorbed phase, the degree of micropore filling of methane adsorbed at 3500 kPa and 298 K, the Henry constant (H) and the adsorption enthalpy ($\Delta_{ads}h_{n^\sigma}$).

The obtained values of H and $\Delta_{ads}h_{n^\sigma}$ showed differences in the adsorbate–adsorbent interaction of the materials studied. Cu-BTC and zeolites 5A and 13X presented high values of H and $\Delta_{ads}h_{n^\sigma}$, indicating an enhanced adsorbent–adsorbate interaction, which could be attributed to their surface properties (especially the presence of open metal sites and cations). Also, it was studied the density of the adsorbed phase of methane at 298 K using the method of the characteristic curves of the Dubinin theory of filling of micropores, and the fraction of micropores filled with CH_4 at the conditions of an ANG tank. It was found that CH_4 is filling almost all the microporosity of the zeolites and the MOF Cu-BTC and MIL-53. However, in ZIF-8 and Maxsorb samples, CH_4 is not filling all the microporosity of the samples. This fact is explained due to the pore size distribution in the Maxsorb sample, and is attributed to the surface properties of ZIF-8, specifically the adsorbate–adsorbent interaction and the pore geometry.

Then, it was showed, in a set of materials with different surface properties, the importance of the adsorbent–adsorbate interaction, as well as the effect of the pore size and geometry for the adsorption capacity of methane at the conditions of an ANG tank.

Acknowledgments

This work was supported by the Spanish Ministry of Economy and Competitiveness (MINECO) through the project PRI-PIBAR-2011-1369; and by the Argentinean Agencies of Science and Technology, FONCYT and CONICET.

Appendix A. Supplementary data

Supplementary data related to this article can be found at http://dx.doi.org/10.1016/j.micromeso.2016.01.002.

References

[1] A.A. García Blanco, A. Vallone, A. Gil, K. Sapag, J. Hydrogen Energy 37 (2012) 14870–14880.
[2] T.A. Makal, J.R. Li, W. Lu, H.C. Zhou, Chem. Soc. Rev. 41 (2012) 7761–7779.
[3] J.P. Mota, in: J.P. Mota, S. Lyubchik (Eds.), Recent Advances in Adsorption Processes for Environmental Protection and Security, Springer, Heidelberg, 2009, pp. 177–192.
[4] V.C. Menon, S. Komarneni, J. Porous Mater. 5 (1998) 43–58.
[5] L. Mentasty, A.M. Woestyn, G. Zgrablich, Adsorpt. Sci. Technol. 11 (1994) 123–133.
[6] S.Y. Zhang, O. Talu, D.T. Hayhurst, J. Phys. Chem. 95 (1991) 1722–1726.
[7] D. Lozano-Castelló, J. Alcañiz-Monge, M.A. de la Casa-Lillo, D. Cazorla-Amorós, A. Linares-Solano, Fuel 81 (2002) 1777–1803.
[8] A. Policicchio, E. Maccallini, R.G. Agostino, F. Ciuchi, A. Aloise, G. Giordano, Fuel 104 (2012) 813–821.
[9] R.B. Rios, F.W.M. Silva, A.E.B. Torres, D.C.S. Azevedo, C.L. Cavalcante Jr., Adsorption 15 (2009) 271–277.
[10] F. Rodríguez-Reinoso, Y. Nakagawa, J. Silvestre-Albero, J.M. Juárez-Galán, M. Molina-Sabio, Micropor. Mesopor. Mater. 115 (2008) 603–608.
[11] C. Solar, F. Sardella, C. Deiana, R. Montero Lago, A. Vallone, K. Sapag, Mat. Res. 11 (2008) 409–414.
[12] C. Solar, A.A. García Blanco, A. Vallone, K. Sapag, in: P. Potocnik (Ed.), Natural Gas, Sciyo, Rijeka, 2010, pp. 205–244.
[13] T. Düren, L. Sarkisov, O.M. Yaghi, R.Q. Snurr, Langmuir 20 (2004) 2683–2689.
[14] M. Eddaoudi, J. Kim, N. Rosi, D. Vodak, J. Wachter, M. ÓKeefe, O.M. Yaghi, Science 295 (2002) 469–472.
[15] Z. Guo, H. Wu, G. Srinivas, Y. Zhou, S. Xiang, Z. Chen, Y. Yang, W. Zhou, M. ÓKeeffe, B. Chen, Angew. Chem. Int. Ed. 50 (2011) 3178–3181.
[16] H. Wu, J.M. Simmons, Y. Liu, C.M. Brown, X.S. Wang, S. Ma, V.K. Peterson, P.D. Southon, C.J. Kepert, H.C. Zhou, T. Yildirim, W. Zhou, Chem. Eur. J. 16 (2010) 5205–5414.
[17] Y. Nakagawa, M. Molina-Sabio, F. Rodríguez-Reinoso, Micropor. Mesopor. Mater. 103 (2007) 29–34.
[18] A.M. Rubel, J.M. Stencel, Fuel 79 (2000) 1095–1100.
[19] S.S.Y. Chui, S.M.F. Lo, J.P.H. Chamant, A.G. Orpen, I.D. Williams, Science 283 (1999) 1148–1150.
[20] L.J. Murray, M. Dincă, J.R. Long, Chem. Soc. Rev. 38 (2009) 1294–1314.
[21] C. Prestipino, L. Regli, J.G. Vitillo, J.G. Bonino, A. Damin, C. Lamberti, A. Zecchina, P.L. Solari, K.O. Kongshaug, S. Bordiga, Chem. Mater. 18 (2006) 1337–1346.
[22] C. Serre, F. Millange, C. Thouvenot, M. Noguès, G. Marsolier, D. Louër, G. Férey, J. Am. Chem. Soc. 124 (2002) 13519–13526.
[23] T. Loiseau, C. Serre, C. Huguenard, G. Fink, F. Taulelle, M. Henry, T. Bataille, G. Férey, Chem. Eur. J. 10 (2004) 1373–1382.
[24] S. Bourrelly, P.L. Llewellyn, C. Serre, F. Millange, T. Loiseau, G. Férey, J. Am. Chem. Soc. 127 (2005) 13519–13521.
[25] K.S.P. Park, Z. Ni, A.P. Côté, J.Y. Choi, R. Huang, F.J. Uribe-Romo, H.K. Chae, M. ÓKeeffe, O.M. Yaghi, Proc. Natl. Acad. Sci. U. S. A. 103 (2006) 10186–10191.
[26] M. Hirscher, B. Panella, B. Schmitz, Micropor. Mesopor. Mater. 129 (2010) 335–339.
[27] J.C. Tan, T.D. Bennet, A.K. Cheethan, Proc. Natl. Acad. Sci. U. S. A. 107 (2010) 9938–9943.

[28] D.M. Ruthven, Principles of Adsorption and Adsorption Processes, John Wiley & Sons, New York, 1984.
[29] H. Marsh, F. Rodríguez-Reinoso, Activated Carbon, Elsevier, Oxford, 2006.
[30] K.S.W. Sing, D.H. Everett, R.A.W. Haul, L. Moscou, R.A. Pierotti, J. Rouquerol, T. Siemieniewska, Pure Appl. Chem. 57 (1985) 603–619.
[31] F. Rouquerol, J. Rouquerol, K. Sing, Adsorption by Powders and Porous Solids, Academic Press, London, 1999.
[32] J. Rouquerol, P. Llewellyn, F. Rouquerol, Stud. Surf. Sci. Catal. 160 (2007) 49–56.
[33] J. Silvestre-Albero, A. Silvestre-Albero, F. Rodríguez-Reinoso, M. Thommes, Carbon 50 (2012) 3128–3133.
[34] D.D. Do, H.D. Do, Carbon 41 (2003) 1777–1791.
[35] K. Murata, M. El-Merraoui, K. Kaneko, J. Chem. Phys. 114 (2001) 4196–4205.
[36] K. Murata, J. Miyawaki, K. Kaneko, Carbon 40 (2002) 425–428.
[37] J. Moellmer, A. Moeller, F. Dreisbach, R. Glaeser, R. Staudt, Micropor. Mesopor. Mater. 138 (2011) 140–148.
[38] J. Alcañiz-Monge, D. Lozano-Castelló, D. Cazorla-Amorós, A. Linares-Solano, Micropor. Mesopor. Mater. 124 (2009) 110–116.
[39] X.S. Chen, B. McEnaney, T.J. Mays, J. Alcañiz-Monge, D. Cazorla-Amorós, A. Linares-Solano, Carbon 35 (1997) 1251–1258.
[40] L. Ming, G. Anzhong, L. Xuesheng, W. Rongshun, Carbon 41 (2003) 579–625.
[41] F. Rodríguez-Reinoso, C. Almansa, M. Molina-Sabio, J. Phys. Chem. B 109 (2005) 20227–20231.
[42] M. Bastos-Neto, A.E.B. Torres, D.C.S. Azevedo, C.L. Cavalcante Jr., Adsorption 11 (2005) 911–915.
[43] M.M. Dubinin, Chem. Rev. 60 (1960) 235–241.
[44] R.F. Cracknell, P. Gordon, K.E. Gubbins, J. Phys. Chem. 97 (1993) 494–499.
[45] K.R. Matranga, A.L. Myers, E.D. Glandt, Chem. Eng. Sci. 47 (1992) 1569–1579.
[46] C. Nguyen, D.D. Do, J. Phys. Chem. B 105 (2001) 1823–1828.
[47] D.D. Do, D. Nicholson, H.D. Do, J. Colloid Interface Sci. 324 (2008) 15–24.
[48] P. Llewellyn, in: N.K. Kanellopoulos (Ed.), Recent Advances in Gas Separation by Microporous Ceramic Membranes, Elsevier, Amsterdam, 2000, pp. 213–230.
[49] A.A. García Blanco, J.C.A. de Oliveira, R. López, J.C. Moreno-Piraján, L. Giraldo, G. Zgrablich, K. Sapag, Colloids Surf. A 357 (2010) 74–83.
[50] T.R. Zeitler, M.D. Allendorf, J.A. Greathouse, J. Phys. Chem. C 116 (2012) 3492–3502.
[51] W. Zhou, H. Wu, M.R. Hartman, T. Yildirim, J. Phys. Chem. C 111 (2007) 16131–16137.
[52] E. Díaz, S. Ordóñez, A. Vega, J. Coca, J. Chromatogr. A 1049 (2004) 139–146.
[53] Y. Sun, C. Liu, W. Su, Y. Zhou, L. Zhou, Adsorption 15 (2009) 133–137.
[54] M. Bastos-Neto, D.V. Canabrava, A.E.B. Torres, E. Rodriguez-Castellón, A. Jiménez-López, D.C.S. Azevedo, C.L. Cavalcante Jr., Appl. Surf. Sci. 253 (2007) 5721–5725.
[55] Y. Peng, V. Krungleviciute, I. Eryazici, J.T. Hupp, O.K. Farha, T. Yildirim, J. Am. Chem. Soc. 135 (2013) 11887–11894.